Permanent dipole moment of tRNA's and variation of their structure in solution

Dietmar Porschke and Jan Antosiewicz
Max-Planck-Institut für biophysikalische Chemie, D-3400 Göttingen, Federal Republic of Germany

ABSTRACT The structure of six different tRNA molecules has been analyzed in solution by electrooptical measurements and by bead model simulations. The electric dichroism measured as a function of the field strength shows that tRNA's are associated with substantial permanent dipole moments, which are in the range of $1 \cdot 10^{-27}$ cm(≡300 D; before correction for the internal directing field). Rotational diffusion time constants of tRNA molecules in their native state at 2°C show a considerable variation. A particularly large value found for $tRNA^{Tyr}$ (50 ns) can be explained by its nine additional nucleotide residues. However, remarkable variations remain for tRNA molecules with the standard number of 76 nucleotide residues ($tRNA^{Phe}$ [yeast] 41.6 ns, $tRNA^{Val}$ [*Escherichia coli*] 44.9 ns, $tRNA^{Glu}$ [*E. coli*] 46.8 ns; $tRNA^{Phe}$ [*E. coli*] 48.3 ns). These variations indicate modulations of the tertiary structure, which may be due to a change of the *L*-hinge angle. Bead models are used to simulate both electric and hydrodynamic parameters of tRNA molecules according to the crystal structure of $tRNA^{Phe}$ (yeast). The asymmetric distribution of phosphate charges with respect to the center of diffusion leads, under the assumption of a constant charge reduction to 15% by ion condensation, to a theoretical dipole moment of $7.2 \cdot 10^{-28}$ cm, which is in reasonable agreement with the measurements. The dichroism decay curve calculated for $tRNA^{Phe}$ (yeast) is also consistent with the measurements and thus the structure in solution and in the crystal must be very similar in this case. However, our measurements also indicate that the structure of some other tRNA's in solution is different, even in cases with the same number of nucleotide residues.

INTRODUCTION

Because the same general structure of tRNA molecules has been found by x-ray analysis of several tRNA species and also of different crystal forms (1–5) it is commonly believed that this structure is maintained in solution. However, the evidence in favor of identical crystal and solution structures remained limited (6–9), partly because the results obtained by the methods available for the analysis of macromolecular structures in solution are not as unambigous as those obtained for crystal structures. Among the various procedures, NMR investigations provide the most detailed informations at the local structure level (10, 11), but small uncertainties in the assignments of the local structure may add up to large uncertainties in the long range structure. Thus, for a complete analysis of macromolecular structures in solution various methods have to be combined. For assignments of long-range structures, rotational diffusion data are known to be most sensitive. In the case of tRNA's, this approach has been mainly used by measurements of fluorescence anisotropies (12–14). Because external dyes have to be coupled to the tRNA's for these measurements in most cases, the results have to be regarded with some caution because of potential ligand-induced changes of the structure. This problem may be avoided by measurements of electric dichroism (15). We have used this method for a comparative analysis of several tRNA species. The experimental results have been analyzed quantitatively by bead model simulations (16).

MATERIALS AND METHODS

All the tRNA's were from Boehringer Mannheim GmbH (FRG). The tRNA samples were dialyzed extensively against several changes of the buffers used for measurements. In all cases the samples were annealed before the measurements by heating to 65°C for 5 min (17). We used the following buffers: A, 1 mM NaCl, 1 mM Na-cacodylate pH 7; B, 10 mM NaCl, 1 mM $MgCl_2$ in addition to components of buffer A; C, 0.5 mM $MgCl_2$ in addition to components of buffer A; D, 2 mM $MgCl_2$ in addition to components of buffer A; CS, 100 μM spermine in addition to components of buffer C; DS, 100 μM spermine in addition to components of buffer D.

The electric dichroism was measured by a pulse generator (18) and an optical detection system (19) described. We have used the strong emissions of a Hanovia mercury/xenon 600 W lamp at 248.2 and 280.4 nm for our investigations. The dichroism transients were first stored on a Tektronix (Beaverton, OR) 7912AD and then transferred to a LSI 11/23, where the signals were averaged and corrected for distortions of the diode grid (20). As shown by tests with quartz-based sinus signals, the accuracy of the recording system was ±1% after corrections. For the

Dr. Antosiewicz's permanent address is Department of Biophysics, Institute of Experimental Physics, University of Warsaw, 02-089 Warsaw, Poland.

final evaluation, the data were sent to the facilities of the Gesellschaft für wissenschaftliche Datenverarbeitung mbH (Göttingen) where an efficient deconvolution routine (21) was used for exponential fitting. The reference curves for deconvolution were measured with identical adjustments of the pulse generator and the detection system; the birefringence of water was used to simulate a fast system response. Stationary values of the dichroism were determined from complete records of electrooptical experiments transiently stored on a Tektronix 7612D; for evaluation of amplitudes by interactive graphic routines the data were transmitted to an LSI 11/23.

Because the electric field pulses do not only induce orientation effects, but also some temperature jump of the solution, the measured rotation time constants had to be corrected. We have used the temperature of the solution before the jump as standard and corrected for the temperature increase by using the usual viscosity/temperature conversion factor (cf. textbooks of biophysical chemistry). The temperature increase was calculated from the amplitude and the length of the field pulse (recorded by a Tektronix 7612D) together with the volume and the resistance of the measuring cell. At the highest field strengths used in the present investigation the temperature was increased in solutions of buffer B by standard pulses of 1.6 μs from 2 to 3.7°C, corresponding to a correction by 6.3%. Test experiments with a fast temperature jump indication system demonstrated that the correction was accurate ± 0.2°C. The temperature before application of electric field pulses was kept constant to ± 0.1°C as measured by a Pt100 sensor inserted in the upper electrode of the cell.

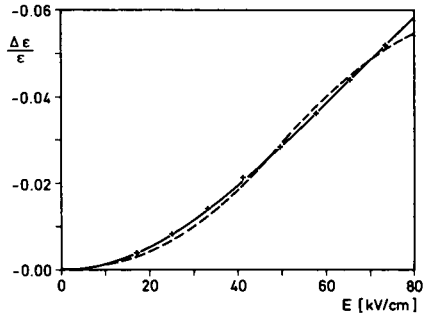

FIGURE 1 Reduced linear dichroism $\Delta\epsilon/\epsilon$ of $tRNA^{Val}$ as a function of the electric field strength E in buffer CS. The continuous line represents a fit according to a permanent dipole model with $\mu = 1.22 \cdot 10^{-27}$ cm and $\Delta\epsilon_\infty/\epsilon = -0.23$, whereas the dashed line represents a least squares fit according to an induced dipole model with a polarizability of $9 \cdot 10^{-34}$ cm^2V^{-1} and $\Delta\epsilon_\infty/\epsilon = -0.072$. The accuracy of the measured $\Delta\epsilon/\epsilon$ data points relative to each other is ~±1% (thus error bars do not exceed size of symbols used for data point presentation); this accuracy is essential for distinction between permanent and induced dipole models. The absolute accuracy is lower (~5%) due to potential errors in absorbance readings etc.

ELECTROOPTICAL MEASUREMENTS

Stationary dichroism indicates permanent dipole moment

Applications of electric field pulses to solutions of tRNA leads to a decrease of the absorbance at 248 nm, when the light is polarized parallel to the field vector ($\Delta A_\parallel < 0$). Stationary values of the absorbance are observed after field pulses of less than a microsecond. Because absorbance changes at the magic angle are negligible (except for buffers of very low salt without a sufficient Mg^{2+} content) and absorbance changes $\Delta A_\perp$ observed for light polarized perpendicular are consistent with $\Delta A_\parallel = -2\Delta A_\perp$ within experimental accuracy, we conclude that the observed effects are due to field-induced alignment of tRNA molecules. A sample data set of the reduced dichroism

$$\frac{\Delta\epsilon}{\epsilon} = \frac{\Delta A_\parallel - \Delta A_\perp}{A}$$

($A \equiv$ isotropic absorbance) is shown in Fig. 1 for the case of $tRNA^{Val}$ as a function of the electric field strength. These data could be fitted at a high accuracy by an orientation mechanism assuming a permanent dipole moment (15). According to the least squares fit, the dipole moment is $1.22 \cdot 10^{-27}$ cm for $tRNA^{Val}$ (in buffer CS). This value has not been corrected for the difference between the external and the internal directing electric field because of the special tRNA structure, which cannot be described by simple standard models for correction.

For comparison we have fitted the same experimental data by an induced dipole model and found that the sum of the squared residuals is much larger (by a factor of ~20) than that obtained for the permanent dipole mechanism. It is also evident by visual inspection that the increase of the reduced dichroism with the electric field strength is not consistent with an induced dipole mechanism (cf. Fig. 1). Nevertheless it is also obvious that the degree of tRNA orientation is far from complete and thus the assignment of the parameters cannot be perfect.

The conclusions described above for the case of $tRNA^{Val}$ have been confirmed by many independent measurements on various tRNA species under different solvent conditions. In virtually all cases the experimental data could be represented more accurately by a permanent dipole model than by an induced dipole model. The observed permanent dipole moments are usually in the range around $10 \cdot 10^{-28}$cm. The limiting values of the dichroism $\Delta\epsilon_\infty/\epsilon$ are always negative; their magnitude is rather variable and depends both on the wavelength and on the details of the buffer composition (cf. Table 1). All $\Delta\epsilon_\infty/\epsilon$ values have been determined by extrapolation of the fitted orientation function to infinite field strengths. Due to this extrapolation, the $\Delta\epsilon_\infty/\epsilon$ values can be defined only at a limited accuracy of ~±25%.

In the case of $tRNA^{Phe}$ (yeast) the dependence of the electrooptical parameters on the buffer composition has been investigated in some more detail. The data measured in the complete absence of free multivalent metal ions, secured by addition of EDTA, can be fitted more accurately by an induced dipole mechanism, whereas a small

TABLE 1 Electrooptical parameters of tRNA's in different buffers at 20°C

	248 *nm*		280 *nm*			248 *nm*		280 *nm*		
	μ_p	$(\Delta\epsilon/\epsilon)_\infty$	μ_p	$(\Delta\epsilon/\epsilon)_\infty$	buffer	μ_p	$(\Delta\epsilon/\epsilon)_\infty$	μ_p	$(\Delta\epsilon/\epsilon)_\infty$	buffer
tRNA A^{fMet}	8.8	−0.44	11	−0.18	D	13	−0.15	15	−0.07	DS
tRNA A^{Glu}	8.7	−0.44	5.7	−0.44	D	—	—	—	—	DS
tRNA A^{Lys}	6.8	−0.78	7.6	−0.34	C	9.2	−0.49	11	−0.22	CS
tRNA A^{Phe} (*E. coli*)	7.7	−0.65	7.9	−0.43	C	11	−0.38	12	−0.25	CS
tRNA A^{Tyr}	7.9	−0.75	7.8	−0.48	C	9.3	−0.58	12	−0.29	CS
tRNA A^{Val}	8.7	−0.41	7.8	−0.37	C	12	−0.23	13	−0.19	CS

μ_p = permanent dipole moment in units of 10^{-27} cm, values are not corrected for internal directing field; $(\Delta\epsilon/\epsilon)_\infty$ = limit value of the reduced dichroism. The accuracy is estimated to be ±10% for the permanent dipole moments and ±25% for the $(\Delta\epsilon/\epsilon)\infty$ values.

amount of Mg^{2+} is sufficient to induce a shift toward a permanent dipole mechanism (cf. Table 2). Apparently the tRNA is without much structure in the complete absence of multivalent ions. As shown by the model calculations given below, the permanent dipole of native tRNA is based on its asymmetric tertiary structure. The electrooptical data indicate that this tertiary structure is formed already at a relatively low Mg^{2+} concentration. We have also studied the pH dependence of the electrooptical parameters of $tRNA^{Phe}$ and found no variation in the pH range from 6.0 to 7.7 within the limits of the experimental accuracy.

The existence of native tRNA structures under our experimental conditions has also been checked by measurements of UV melting curves in buffer B. For all tRNA molecules used in the present investigation, an increase of the absorbance at 260 nm was observed only for temperatures >40°C. The main part of the absorbance increase corresponding to denaturation was found at temperatures >70°C. This result supports our conclusion that the tRNA's are in their native structure under the conditions of our electrooptical measurements.

TABLE 2 Electrooptical data of $tRNA^{Phe}$ (yeast) as a function of the Mg^{2+} concentration in buffer A

Components added to buffer A	μ_p (10^{-28} cm)	$(\Delta\epsilon/\epsilon)_\infty$	t
			°C
100 μM EDTA	$(12 \cdot 10^{-33})$*	−0.19	20
—	17	−0.27	20
50 μM Mg^{2+}	9.3	−0.45	2
170 μM Mg^{2+}	9.8	−0.37	20
200 μM Mg^{2+}	11.1	−0.38	2
1 mM Mg^{2+}	8.3	−0.49	2
5 mM Mg^{2+}	6.4	−0.58	2

μ_p = permanent dipole moment; $(\Delta\epsilon/\epsilon)_\infty$ = limit dichroism at 248 nm; t = temperature.
*Polarizability in (cm^2 V^{-1}), in this case the data were fitted more accurately by an induced dipole mechanism.

Dichroism decay curves show variation of structure for different tRNA's

Because of the rather fast rotational diffusion of tRNA molecules, the quantitative evaluation of dichroism decay curves requires an efficient deconvolution routine. Because our deconvolution procedure (21) proved to be efficient and reliable, the decay curves were not measured at maximal time resolution of our apparatus, but at a slightly reduced resolution with the benefit of an improved signal to noise ratio. As shown by the example in Fig. 2, the dichroism decay curves of tRNA can be fitted by single exponentials at high accuracy. Usually the decay curves were recorded at 248 nm at a concentration ~1 μM of tRNA molecules. The decay time constants recorded in this range are not dependent on the nucleotide concentration (cf. Fig. 3). Corresponding results have been obtained for all the tRNA species used in this investigation. In the range of electric field strengths E from 35 to 65 kV/cm, where decay time constants τ_d could be measured at a sufficient accuracy, the τ_d values

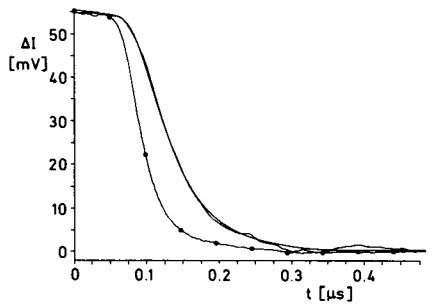

FIGURE 2 Dichroism decay curve of yeast $tRNA^{Phe}$ measured at 2°C in buffer B (average of 10 shots). The line marked by small circles represents the reference curve used for deconvolution and the line without noise represents a least squares fit with an exponential time constant of 39 ns. The time constants given elsewhere in the text, tables and figures were corrected for the temperature jump effect (cf. text).

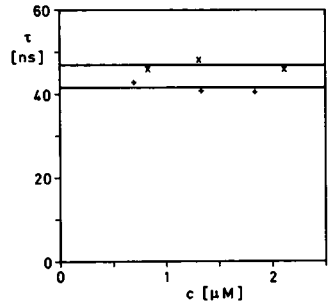

FIGURE 3 Dichroism decay time constant for $tRNA^{Glu}$ (×) and yeast $tRNA^{Phe}$ (+) as a function of the tRNA concentration (2°C, buffer B).

were not dependent on E. Furthermore, the wavelength of the light used for the measurements (248 or 280 nm) did not influence the τ_d values within the experimental accuracy of ±3%. The decay time constants obtained in buffer B, which are compiled in Table 3, demonstrate a quite remarkable variation, even for tRNA species with the same number of nucleotide residues.

Because this variation may be explained by partial denaturation of the tRNA tertiary structure, we have studied the dependence of the decay time constant on the buffer composition. For technical reasons electrooptical experiments are usually performed at relatively low salt concentrations, which might lead to some denaturation. However, independent measurements show that the tertiary structure of tRNA starts to be disrupted at much lower salt concentrations than that of buffer B. For example, the dichroism decay time constant τ of $tRNA^{Phe}$ (yeast) is 102 ns in buffer B with 200 μM EDTA and 41.2 ns in buffer B with 50 μM $MgCl_2$. Obviously, the relatively slow rotational diffusion observed in the presence of EDTA reflects the denatured, extended form of the tRNA. This result is consistent with UV melting profiles. The rather small $\Delta\epsilon_\infty/\epsilon$ value (cf. Table 2) associated with the denatured structure appears to be in contrast with the existence of an extended form; however, single stranded nucleotide chains do not necessarily show large $\Delta\epsilon_\infty/\epsilon$ values (cf. data for poly[C] given in reference 22). Addition of a rather low amount of Mg^{2+} to the denatured tRNA leads to the formation of the compact, native form. A further increase of the Mg^{2+} concentration does not lead to a further change of the τ value, until an increase of τ is observed at high Mg^{2+} levels, which apparently reflects the formation of aggregates.

In the range of electric field strengths, where time constants could be measured at a sufficient accuracy (35–65 kV/cm), the risetime constants were larger by a factor of ~2 than the decay time constants. This result clearly confirms the conclusion given above on a dominant contribution of a permanent dipole moment, because induced dipole moments do not show a slower rise than decay of the dichroism (15). A comparison with the time constants associated with ion polarization of DNA double helices (23) leads to a further support of this argument. According to a preliminary analysis of the rise curves at different electric field strengths, the rise curves apparently do not always completely approach the limit at low field strength, which is expected for permanent dipoles according to theory. The extrapolation of time constants to field strengths $E = 0$ from measurements in the range $E > 35$ kV/cm is rather difficult and requires data of particularly high accuracy. It should be expected that there is some contribution to tRNA orientation due to ion polarization in addition to that resulting from its permanent dipole moment. The magnitude of this contribution remains to be established.

TABLE 3 Average rotation time constants in nanoseconds

	2°C	20°C
Tyr	50.0	28.1
Phe (*E. coli*)	48.3	27.2
Glu	46.8	26.3
fMet	45.1	25.4
Val	44.9	25.3
Phe (yeast)	41.6	23.4

tRNA's in 10 mM NaCl, 1 mM $MgCl_2$, 1 mM Na-cacodylate pH 7.0. The values given at 20°C have been calculated from the values measured at 2°C using the temperature–viscosity conversion factor 1.777. The estimated accuracy of the time constants is ±3%.

BEAD MODEL SIMULATIONS

General

Bead models (16) are used to simulate hydrodynamic parameters of objects, which cannot be adequately represented by simple geometric bodies like spheres or ellipsoids. These simulations are also required to define dipole moments for objects with a net charge, because in this case dipole moments must be referred to the "center of diffusion" (cf. reference 24).

Construction of bead models

We start from the known crystal structure of $tRNA^{Phe}$ in the form published by Ladner et al. (25) and substitute each nucleotide by one bead. The center of each bead corresponds to the mass center of the nucleotides, which have been calculated under the assumption of equal masses of all atoms. The distance of the nucleotide atom, which is most remote from the mass center, is defined as

bead radius; we use the average value found for the four nucleotides as a starting value, because only a single bead radius is allowed for simulations with overlapping beads (16). This starting value was corrected for, e.g., the contribution of solvation by a procedure based on experimental data obtained for DNA. First a bead model is constructed for the B-DNA dodecamer of Drew et al. (26) using the procedure described above. For a comparison with available experimental data, the dodecamer is then elongated by simple addition of dodecamer helix blocks up to a length of 43 bp. The bead positions in the 43 bp fragment were obtained from those of the dodecamer by translation of the first 10 pairs of beads along the helix axis, until the first pair covered approximately the position of the 11th pair (both are GC). We have neglected the rotation required by the fact that full helix turn comprises 10.4 and not 11 bp, partly because this detail will hardly be important for simulations of hydrodynamics and also because the junction points in our model are not distorted according to visual inspection. The translation was repeated four times and the beads corresponding to the first 43 bp were used for simulations. The bead radius of this model was fitted to the experimental rotation time constant of 102 ns (reference 27); the optimal value is $r = 6.45$ Å. We assume that the correction $\Delta r = 1$ Å resulting from this fit also applies for tRNA beads and arrive at a bead radius for tRNA $r = 6.39$ Å. Obviously this value should be regarded as approximate. A view of a $tRNA^{Phe}$ (yeast) bead model is shown in Fig. 4.

Hydrodynamic simulations

The resistance, diffusion and alignment tensors were calculated as described previously (16, 28). Volume corrections were applied as discussed in reference 16. Finally, dichroism decay curves were evaluated according to the procedure of Wegener et al. (29) using the electric and optical parameters described below.

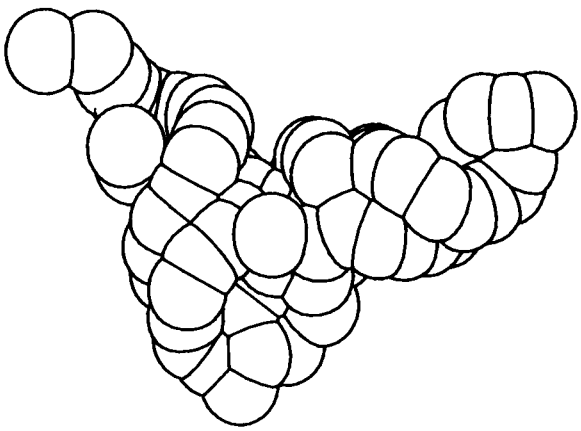

FIGURE 4 Bead model of yeast $tRNA^{Phe}$ (bead radius 6.39 Å).

Electric moments

Initial values of dipole moments were calculated according to the standard definition

$$\mu = \Sigma\, q_i r_i,$$

where q_i and r_i are the charge and the position vector of atom i in the coordinate system of the crystal structure data. Because tRNA's bear net charges, dipole moments with physical meaning must be referred to the center of diffusion according to

$$\mu_{CD} = \mu - R_{CD}\, \Sigma\, q_i,$$

where R_{CD} is the position of the vector of the center of diffusion in the initial coordinate system.

We have calculated dipole moments for three different models. First, we considered only phosphate charges in our calculation and assumed that, because of ion condensation, each phosphate is associated with 15% of the electron charge. In a second model we included three magnesium ions, which are known to be strongly bound at given coordination sites (30) (the sites are denoted by the numbers of the adjacent phosphates in the nucleotide chain; 1. site: P1 + P2; 2. site: P10; 3. site: P20 + 21). In the third model we considered three additional Mg^{2+}-ions, which are known to be less strongly bound (30) (4. site: P19; 5. site: P37; 6. site: P50 + P51 + P59 + P60). The positions of all Mg^{2+} ions were assumed to coincide with the phosphates of their coordination site and thus the resulting charges were assigned to the position of the corresponding phosphates. When a single phosphate was close to the Mg^{2+} ion, its charge was counted as positive. Because the effective phosphate charges are known to be reduced due to counterion condensation, we have assumed a corresponding effect for phosphate-Mg complexes. In all cases we have assumed a reduction to 15% of the charge in the unshielded state. When a Mg^{2+} ion is in contact with two adjacent phosphates according to the crystal structure, their charges were assigned to zero. According to our experimental results the polarizability of tRNA is relatively small and may be neglected. (For the simulations on the 43 bp DNA fragment, we considered only the polarizability along the helix axis and assigned the value according to experimental data [31].)

Absorption coefficient tensor

The directions of the transition dipole moments contributing to the nucleotide absorbance in the range around 260

nm were taken from Rizzo and Schellman (32). According to these authors the directions can be given by the positions of ring atoms as follows: adenine C4 → C5, guanine C8 → C2, cytosine C4 – N1, and thymine N1 – C5. For the other bases found in tRNA we used the transition dipole moment of those standard bases, which are most closely related according to their chemical structure (e.g., uracil is assumed to be equivalent to thymine). For a simulation at 280 nm we used a direction of the transition dipole moment for guanine from C2 to C6 (cf. reference 32), whereas the corresponding directions for the other bases were assumed to be identical at 260 and 280 nm. The components of the local absorption tensors corresponding to each nucleotide were transformed to the coordinate system of the crystal structure and summed up to the absorption tensor of the whole macromolecule. The result was checked by summation starting from different initial coordinate systems.

Limiting reduced dichroism

First the eigenvalues are calculated for the alignment tensor (29). In the limit of an infinitely high external electric field, the macromolecules are aligned such that the eigenvector of the alignment tensor corresponding to its maximal eigenvalue is parallel to the field. Thus, the components A_{xx}, A_{yy}, and A_{zz} of the absorption tensor have to be calculated in the coordinate system of the principal axes of the alignment tensor. Finally, the limiting dichroism is calculated by

$$\frac{\Delta\epsilon_\infty}{\epsilon} = 3[A_{zz} - (A_{xx} + A_{yy})/2]/tr(A),$$

where $tr(A)$ is the trace of the absorption tensor.

Comparison of theoretical and experimental results

The calculated dichroism decay curves are composed of five exponentials (29), which could not be resolved in the experiments. Because the experimental data were fitted by single exponentials, we used a corresponding least squares procedure to fit single exponentials to the calculated dichroism decay curves. In general the fitted single exponential curves could hardly be distinguished from the exact simulation data except in difference curves or difference correlation plots. Thus, at the given noise of the experimental data it is virtually impossible to extract more than single exponentials.

Results

The bead models have been used to simulate permanent dipole moments μ_p, limiting values of the linear dichroism $\Delta\epsilon_\infty/\epsilon$ corresponding to complete alignment in the electric field and average rotational diffusion time constants $\bar{\tau}$. In all cases the data have been simulated for different numbers of bound Mg^{2+} ions. As shown in Table 4 for $tRNA^{Phe}$ (yeast), the permanent dipole moment decreases with the number of bound Mg^{2+} ions, whereas the other parameters remain almost unaffected. The value of the permanent dipole moment is, of course, strongly dependent on the degree of charge compensation by counterions, which is not known exactly for the case of tRNA. We have based our calculations on effective charges corresponding to 15% of the total nominal charges, which has been estimated from polyelectrolyte theory (33), and arrive at calculated dipole moments, which are rather close to the experimental ones. A simulation of the limit dichroism in the wavelength range ~280 nm (transition dipole moments cf. above) provided the same result as that obtained for the range ~260 nm, within the limits of accuracy. Probably the different values for $\Delta\epsilon_\infty/\epsilon$ measured in some cases for 248 and 280 nm (cf. Table 1) are due to a contribution of n-π transitions, which have not been considered in our absorption coefficient tensor.

DISCUSSION

Although tRNA's have been analyzed by virtually all methods available (34, 35), a detailed analysis by electrooptical measurements has not been presented yet. Apparently, this is mainly due to technical reasons because the rotational diffusion of tRNA is rather fast and is relatively difficult to resolve with standard electrooptical facilities. Furthermore, the optical and the electrical anisotropy of tRNA is relatively small, when compared with DNA double helices, for example. Thus, only few reports appeared on this subject (36, 37). We have been able to measure electrooptical data for various tRNA's at a particularly high accuracy by application of relatively high electrical field pulses with short rise and decay times and by evaluation of the transients with an efficient deconvolution technique. Our experimental data have been collected at much lower tRNA concentrations than

TABLE 4 Electrooptical parameters calculated for $tRNA^{Phe}$ (yeast), μ_p permanent dipole moment in units of 10^{-27} cm, $\Delta\epsilon_\infty/\epsilon$ limit dichroism calculated for the wavelength range around 260 nm, $\bar{\tau}$ average rotational diffusion time constant in nanoseconds at 2°C

Mg ions	μ_p	$\Delta\epsilon_\infty/\epsilon$	$\bar{\tau}$
0	7.20	−0.373	48.3
3	6.45	−0.407	50.8
6	5.07	−0.387	48.3

have been used previously for measurements of the optical Kerr effect (37), for example. Thus, our results are not perturbed by intermolecular interactions.

The analysis of the stationary dichroism measured as a function of the electric field strength clearly shows the existence of a permanent dipole moment. This conclusion is supported by an analysis of the dichroism rise curves. Finally, the theoretical analysis of the tRNA structure by bead models shows that a considerable permanent dipole moment must be expected due to the assymetry of the tertiary structure. Thus, the existence of a permanent dipole moment for tRNA is beyond any doubt. Obviously, tRNA as a polyelectrolyte should also have a strong polarizability, but at least under our various experimental conditions the permanent moment is dominant in the native conformation.

In a future analysis it may be attempted to characterize the relative magnitude of the permanent to the induced dipole moment. However, such an analysis would require experimental data of increased accuracy, which are not yet available. At present it cannot be excluded that the permanent dipole moment derived from our experimental data is too large by 20%, for example, due to the fact that a tRNA polarizability has not been considered in our evaluation. A corresponding uncertainty is associated with our model calculations. The assumption of a constant reduction of phosphate charges to 15% by counterions has been useful as a first approximation, but probably does not exactly reflect the true charge distribution for the rather complex tRNA tertiary structure. However, the approximate agreement of experimental and calculated results suggests that the model used for the calculation is rather close to reality.

It is tempting to speculate about a potential biochemical function of the permanent tRNA dipole moment. The dipole moment may be useful, for example, during binding of tRNA's to ribosomes: it may favor a correct orientation of tRNA for insertion into the ribosomal cleft.

Usually the global structure of tRNA molecules in solution is regarded to be constant and equivalent to that found in crystals by x-ray crystallography. Our measurement of the dichroism decay time constants demonstrate that the structure of different tRNA's with the standard number of 76 nucleotide residues are not identical in solution. According to our experimental tests, these tRNA's are in their native tertiary structure under the conditions of our measurements. The variation of the rotational diffusion time constants may be due to changes of the *L*-hinge angle. Different hinge angles have been observed in the crystal structures of $tRNA^{Phe}$ (yeast) (1, 2, 25) and $tRNA^{Asp}$ (yeast) (5). Moras et al. (5) attribute the special structure of $tRNA^{Asp}$ to base pairing of its anticodon and suggest that a corresponding conformation change induced by base pairing at the anticodon may be general for tRNA molecules (cf. reference 38). At present this problem is analyzed in more detail by further electrooptical measurements. It should be mentioned that the differences in the electrooptical data, which have been described above, need not be due to differences in the tRNA equilibrium conformations, but may also be explained by different degrees of flexibility, for example, at the *L*-hinge angle, the CAA end, and the anticodon loop.

In the case of $tRNA^{Phe}$ (yeast) the time constant derived from the dichroism decay may be compared with time constants evaluated from measurements of the fluorescence anisotropy. Claesens and Rigler (39) reported a time constant of 19 ns at 20°C for the "native" tRNA, whereas Striker et al. (40) assigned three exponentials (0.39, 9.9, and 28.1 ns at 10°C). Apparently, the fast components are associated with local motions of wybutine; these appear with a relatively small amplitude for the "native" tRNA formed in the presence of Mg^{2+} and a much larger amplitude for the "denatured" conformation induced in the absence of Mg^{2+}, where fast components have also been identified by Claesens and Rigler. The time constant of the slow component observed in the fluorescence anisotropy decay is close to that derived from the dichroism decay, which is consistent with expectation. However, the accuracy of the rotational diffusion time constants derived from the fluorescence anisotropy decay is limited because of the relatively short decay time of the wybutine fluorescence.

The present investigation very clearly shows the high potential of quantitative electrooptical investigations for the characterisation of macromolecular structures in solution but also illustrates some limitations. Among the major advantages of electrooptical methods is the high sensitivity of dichroism (or birefringence) time constants with respect to molecular dimensions, the readily accessible information on the orientation of chromophores and the fact that measurements do not require large amounts of material. Furthermore, it is not necessary to introduce any spectroscopic labels, which may perturb the structure. However, a major problem associated with electrooptical measurements is the restriction to relatively low salt concentrations. Another problem may come from a special coupling of hydrodynamic, electric, and optical properties, which may cause confusion in the case of molecules with a complex shape and without symmetry like tRNA's. In such cases quantitative evaluations of electrooptical data are possible, when there is independent information on the molecular structure, as shown in the present investigation for the example of $tRNA^{Phe}$. Then, it is possible to check overall molecular dimensions, the relative positions of charged residues and of chromophores with a particularly high accuracy. Thus, electrooptical measurements can be particularly useful for a comparison of structures in crystals and in solution. Furthermore,

quantitative electrooptical procedures should be very useful for the analysis of conformation changes induced by, e.g., ligand binding.

For our computations we used the facilities of the Gesellschaft für wissenschaftliche Datenverarbeitung m.b.H., Göttingen.

Received for publication 18 October 1989 and in final form 2 April 1990.

REFERENCES

1. Quigley, G. J., N. C. Seeman, A. H. J. Wang, F. L. Suddath, and A. Rich. 1975. Yeast phenylalanine transfer RNA: atomic coordinates and torsion angles. *Nucl. Acids. Res.* 2:2329–2341.
2. Jack, A., J. E. Ladner, and A. Klug. 1976. Crystallographic refinement of yeast phenylalanine transfer RNA at 2.5 Å resolution. *J. Mol. Biol.* 108:619–649.
3. Schevitz, R. W., A. D. Podjarny, N. Krishnamachari, J. J. Hughes, P. B. Sigler, and J. L. Sussman. 1979. Crystall structure of an eukariotic initiator tRNA. *Nature (Lond.).* 278:188–190.
4. Woo, N. H., B. A. Roe, and A. Rich. 1980. Three-dimensional structure of *Escherichia coli* initiator $tRNA_f^{Met}$. *Nature (Lond.).* 286:346–351.
5. Moras, D., A. C. Dock, P. Dumas, E. Westhof, P. Romby, J. P. Ebel, and R. Giege. 1986. Anticodon–anticodon interaction induces conformational changes in tRNA: Yeast $tRNA^{Asp}$, a model for tRNA-mRNA recognition. *Proc. Natl. Acad. Sci. USA.* 83:932–936.
6. Langlois, R., S. H. Kim, and C. R. Cantor. 1975. A comparison of the fluorescence of the Y base of yeast $tRNA^{Phe}$ in solution and in crystals. *Biochemistry.* 14:2554–2558.
7. Chen, N. C., R. Giege, R. C. Lord, and A. Rich. 1975. Raman spectra and structure of yeast phenylalanin transfer RNA in the crystalline state and in solution. *Biochemistry.* 14:4385–4391.
8. Romby, P., D. Moras, P. Dumas, J. P. Ebel, and R. Giege. 1987. Comparison of the tertiary structure of yeast $tRNA^{Asp}$ and $tRNA^{Phe}$ in solution. Chemical modification study of the bases. *J. Mol. Biol.* 195:193–204.
9. Kim, S. H. 1978. Crystal structure of yeast $tRNA^{Phe}$: its correlation to the solution structure and functional implications. *In* Transfer RNA. S. Altman, editor. MIT Press, Cambridge, MA. 248–293.
10. Schimmel, P. R., and A. G. Redfield. 1980. Transfer RNA in solution: selected topics. *Annu. Rev. Biophys. Bioeng.* 9:181–221.
11. Heerschap, A., J. R. Mellema, H. G. J. M. Janssen, J. A. L. I. Walters, C. A. G. Haasnoot, and C. W. Hilbers. 1985. Imino-proton resonances of yeast $tRNA^{Phe}$ studies by two-dimensional nuclear Overhauser enhancement spectroscopy. *Eur. J. Biochem.* 149:649–655.
12. Tao, T., J. H. Nelson, and C. R. Cantor. 1970. Conformational studies of transfer ribonucleic acid. Fluorescence lifetime and nanosecond depolarization measurements on bound ethidium bromide. *Biochemistry.* 9:3514–3524.
13. Rigler, R., and W. Wintermeyer. 1983. Dynamics of tRNA. *Annu. Rev. Biophys. Bioeng.* 12:475–505.
14. Wells, B. D., and J. R. Lakowicz. 1987. Intensity and anisotropy decays of the Wye base of yeast $tRNA^{Phe}$ as measured by frequency-domain fluorometry. *Biophys. Chem.* 26:39–43.
15. Frederique, E., and C. Houssier. 1973. Electric Dichroism and Electric Birefringence. Clarendon Press, Oxford. 219 pp.
16. Garcia de la Torre, J., and V. A. Bloomfield. 1981. Hydrodynamic properties of complex, rigid, biological macromolecules: theory applications. *Q. Rev. Biophys.* 14:81–139.
17. Grosjean, H. J., D. G. Söll, and D. M. Crothers. 1976. Studies of the complex between transfer RNAs with complementary anticodons. I. Origins of enhanced affinity between complementary tripletts. *J. Mol. Biol.* 103:499–519.
18. Grünhagen, H. H. 1974. Entwicklung einer E-Feldsprung-Apparatur mit optischer Detektion und ihre Anwendung auf die Assoziation amphiphiler Elektrolyte. Ph.D. Thesis. Universität Braunschweig.
19. Porschke, D. 1980. Structure and dynamics of a tryptophanepeptide-polynucleotides complex. *Nucleic Acids Res.* 8:1591–1612.
20. Programmable Digitizer 7912AD, Instruction Manual. 1985. Tektronix, Inc., Beaverton, Oregon.
21. Porschke, D., and M. Jung. 1985. The conformation of single stranded oligonucleotides and of oligonucleotide-oligopeptide complexes from their rotation relaxation in the nanosecond time range. *J. Biomol. Struct. & Dyn.* 2:1173–1184.
22. Porschke, D. 1976. Threshold effects observed in conformation changes induced by electric field pulses. *Biopolymers.* 15:1917–1928.
23. Porschke, D. 1985. The mechanism of ion polarisation along DNA double helices. *Biophys. Chem.* 22:237–247.
24. Antosiewicz, J., and D. Porschke. 1989. An unusual electrooptical effect observed for DNA fragments and its apparent relation to a permanent electric moment associated with bent DNA. *Biophys. Chem.* 33:19–30.
25. Ladner, J. E., A. Jack, J. D. Robertus, R. S. Brown, D. Rhodes, B. F. C. Clark, and A. Klug. 1975. Atomic co-ordinates for yeast phenyalanine tRNA. *Nucleic Acids Res.* 2:1629–1637.
26. Drew, H. R., R. M. Wing, T. Takano, C. Broka, S. Tanaka, K. Itakura, and R. Dickerson. 1981. Structure of a B-DNA dodecamer: conformation and dynamics. *Proc. Natl. Acad. Sci. USA.* 78:2179–2183.
27. Porschke, D. 1986. Structure and dynamics of double helices in solution: Modes of DNA bending. *J. Biomol. Struct. & Dyn.* 4:373–389.
28. Antosiewicz, J., and D. Porschke. 1988. Turn of promotor DNA by cAMP receptor protein characterized by bead model simulation of rotational diffusion. *J. Biomol. Struct. & Dyn.* 5:819–837.
29. Wegener, W. A., R. M. Dowben, and V. J. Koester. 1979. Time-dependent birefringence, linear dichroism, and optical rotation resulting from rigid-body rotational diffusion. *J. Chem. Phys.* 70:622–632.
30. Teeter, M. M., G. J. Quigley, and A. Rich. 1980. Metal ions and transfer RNA. *In* Nucleic Acid-Metal Ion Interactions. T. G. Spiro, editor. John Wiley & Sons Ltd., New York. 145–177.
31. Diekmann, S., W. Hillen, M. Jung, R. D. Wells, and D. Porschke. 1982. Electric properties and structure of DNA restriction fragments from measurements of the electric dichroism. *Biophys. Chem.* 15:157–167.
32. Rizzo, V., and J. Schellman. 1984. *Biopolymers.* 23:435–470.
33. Manning, G. 1978. The molecular theory of polyelectrolyte solutions with applications to the electrostatic properties of polynucleotides. *Quart. Rev. Biophys.* 11:179–246.

34. Schimmel, P. R., D. Söll, and J. N. Abelson, editors. 1979. Transfer RNA: Structure, Properties, and Recognition. Cold Spring Harbor Laboratory, USA. 577 pp.

35. Altman, S., editor. 1978. Transfer TNA. MIT Press, Cambridge, MA. 356 pp.

36. Thompson, M. R., R. C. Williams, and C. H. O'Neal. 1978. Studies on proteins and tRNA with transient electric birefringence. *Biophys. J.* 24:264–266.

37. Dobek, A., and J. Deprez. 1986. Optical Kerr effect induced by picosecond light pulses in tRNA solutions. *J. Colloid Interf. Sci.* 111:75–93.

38. Labuda, D., G. Striker, and D. Porschke. 1984. Mechanism of codon recognition by transfer RNA and codon-induced tRNA association. *J. Mol. Biol.* 174:587–604.

39. Claesens, F., and R. Rigler. 1986. Conformational dynamics of the anti-codon loop in yeast $tRNA^{Phe}$ as sensed by the fluorescence of wybutine. *Eur. Biophys. J.* 13:331–342.

40. Striker, G., D. Labuda, and M. del Carmen Vega-Martin. 1989. The three conformations of the anticodon loop of Yeast $tRNA^{Phe}$. *J. Biomol. Struct. & Dyn.* 7:235–255.